Clim Dyn
DOI 10.1007/s00382-012-1474-1

The observed teleconnection between the equatorial Amazon and the Intra-Americas Seas

V. Misra · S. M. DiNapoli

Received: 20 February 2012 / Accepted: 25 July 2012

Abstract Using observations of rainfall and SST analysis it is shown that there is a robust relationship with two-season lag between the austral summer (December–January–February [DJF]) Equatorial Amazon (EA) rainfall and the following boreal summer season (June–July–August [JJA]) Intra-Americas Seas (IAS) Sea Surface Temperature Anomalies (SSTA). It is observed that in wetter than normal austral summer seasons over EA, the SSTA in the IAS are cooler than normal in the following JJA season. This teleconnection also manifests in the ocean heat content of the IAS region. Our analysis indicates that the net surface heat flux into the ocean (particularly the surface longwave and the shortwave radiative fluxes) dictates the strongest influence on the JJA Caribbean SSTA, the core region of the IAS where the observed teleconnection with EA rainfall is strongest. This study also finds that this teleconnection is in fact a manifestation of the remote ENSO forcing on the Caribbean SSTA through its modulation of the EA rainfall anomalies. In a wet DJF year over EA, the Atlantic Inter-Tropical Convergence Zone (ITCZ) moves further southward than climatology. This causes the dry limb of the associated overturning circulation of the Atlantic ITCZ to reside over the Caribbean Sea region in the subsequent March–April–May and JJA seasons. As a result of this large-scale descent in the wet DJF year over EA, there is a net decrease in the heat flux into the ocean from increased emission of surface longwave radiation in the presence of anomalously dry atmosphere. In a dry DJF year over EA the Atlantic ITCZ is nearly co-located in the core region of the IAS, which is northward than the climatological location, resulting in the descending limb of the overturning location to be located further south of the Caribbean Sea leading to warmer SSTA.

V. Misra (✉)
Department of Earth, Ocean and Atmospheric Science, Florida State University, Tallahassee, FL, USA
e-mail: vmisra@fsu.edu

V. Misra · S. M. DiNapoli
Center for Ocean-Atmospheric Prediction Studies, Florida State University, Tallahassee, FL, USA

1 Introduction

The Intra Americas Seas (IAS), which comprise of the Gulf of Mexico, the Caribbean Sea and parts of the northwestern tropical Atlantic Ocean, are considered to be part of the warm pool of the western hemisphere (Wang and Enfield 2001), which hosts the second largest body of very warm water (≥28.5 °C) on Earth. A small fraction of this Western Hemisphere Warm Pool (WHWP) also resides in the northeast tropical Pacific Ocean, which however will not be part of this study.

There is growing observational evidence of the influence of the IAS on the warm season precipitation over the Caribbean region, Central America, the southeast Pacific, and over several regions in the United States including the northwest, the southeast, and the Great Plains region (Wang et al. 2006, 2008; Wang and Lee 2007; Misra et al. 2011). The variability of the IAS is associated with the variability of the North Atlantic Subtropical High (NASH). The NASH in turn modulates the moisture transport into the continental regions of Mesoamerica and parts of the United States through its influence on the Caribbean low-level jet and the Great Plains low level jet that includes the southerly flow from the Gulf of Mexico (Wang et al. 2006; Wang and Lee 2007; Rauscher et al. 2010; Chan et al. 2011; Misra et al. 2009). Furthermore, Wang and Lee (2007) showed that the IAS induced atmospheric changes of vertical shear and convective instability

Published online: 07 August 2012

are the primary mechanisms by which the IAS controls Atlantic tropical cyclones. Therefore the importance of the variability of the IAS cannot be over emphasized. In this paper we examine the teleconnection at interannual scales between the boreal summer season Caribbean Sea Surface Temperature Anomalies (SSTA) and the preceding austral summer season rainfall anomalies over the Equatorial Amazon.

The teleconnection between the Amazon and the IAS is referred in several studies (Enfield and Mayer 1997; Saravanan and Chang 2000; Wang 2002; Chiang and Sobel 2002; Mestas-Nunez and Enfield 2001; Munoz et al. 2010). Many of these studies treat Amazon convection as a conduit for the El Niño and the Southern Oscillation (ENSO) influence on tropical North Atlantic Ocean. Furthermore many of these studies dwell on the variability of the SSTA in the boreal spring season over the northwestern tropical Atlantic Ocean, which is part of the IAS. Theoretical and modeling studies have suggested that this region has self regulating meridional circulations in the atmosphere (Hadley cell) that are inter-hemispheric. These circulations are generated by diabatic heat release in the atmosphere, whose source alternates between the Amazon in boreal winter to the IAS in the boreal summer (Lee et al. 2009; Wang et al. 2010). Wang (2002) also suggested that Amazonian convective activity provides a cross-hemispheric connection to the NASH (or Bermuda high) through a Hadley-type circulation. In addition, freshwater discharge from large river systems like the Amazon and Orinoco can potentially modulate tropical Atlantic SST. Foltz and McPhaden (2009) indicate that seasonal variations of the barrier layer thickness (also dictated by the Amazon discharge) exert considerable influence on SST over central tropical north Atlantic. In the modeling study of Vizy and Cook (2010) it is suggested that fresh water discharges from the Amazon and Orinoco river mouths affect the tropical Atlantic storm activity. Munoz et al. (2010) identify that ENSO affects the Gulf of Mexico and the Caribbean Sea in the opposite manner to generate a SST dipole pattern in the boreal spring season within the IAS region.

In this study we show a teleconnection between the Equatorial Amazon (EA; 7°S–7°N and 65°W–50°W) rainfall variation in austral summer season (December–January–February [DJF]) and the subsequent IAS sea surface temperature variations in boreal summer season (June–July–August [JJA]). It may be noted that EA is well known for its teleconnection with the ENSO variations (Liebmann and Marengo 2001).

2 Data

We make use of the Climate Research Unit version 3.0 (CRU3.0; Mitchell and Jones 2005) for the period 1950–2004 for monthly mean rainfall. This dataset is available on a grid resolution of 0.5°. We also supplement this rainfall data set with NOAA's Climate Prediction Center Merged Analysis of Precipitation (CMAP; Xie and Arkin 1996) as it covers both ocean and land unlike CRU3.0, which is only over land. The observed monthly mean SST is obtained from the NOAA Extended Reconstructed SST version 3 (ERSSTv3; Smith et al. 2008). We also make use of the National Centers for Environmental Protection (NCEP) Climate Forecast System Reanalysis (CFSR; Saha et al. 2010) for the atmospheric and oceanic variables and surface fluxes. This reanalysis is available for the period 1979 to the present at about 30 km grid resolution globally. Despite the relatively shorter period of coverage of CFSR compared to either CRU3.0 or ERSSTv3, we were inclined to use this reanalysis for its higher spatial resolution and an improved (and modern) version of the analysis model with the novel concept of including the effect of coupled ocean–atmosphere process in the data assimilation (Saha et al. 2010). However, most importantly, CFSR offers the availability of dynamically and physically consistent sub-surface ocean temperature data in addition to atmospheric data.

3 Methodology

In this section we delineate a methodology to diagnose the forcing terms for the development of the SSTA following Kang et al. (2001). This is used to understand the physical processes involved in developing the SSTA in JJA over the IAS. The SSTA equation may be written as:

$$\frac{\partial T'}{\partial t} = -u_c\frac{\partial T'}{\partial x} - v_c\frac{\partial T'}{\partial y} - u'\frac{\partial T}{\partial x} - v'\frac{\partial T}{\partial y} - w_c\frac{\partial T'}{\partial z} - (w - w_c)\frac{\partial T}{\partial z} - Q' \quad (1)$$

where T' is the SSTA, u_c and v_c, are climatological zonal and meridional currents, w_c is the climatological vertical velocity. The prime quantities are the corresponding anomalous variables. Q' in the above equation refers to the residual terms of fluxes and diffusion. It may be noted that the above equation is not the same as the one used in CFSR, especially as the SST and surface salinity in CFSR are restored to observations by nudging during the data assimilation. However, the aim here is not to seek an SST budget but to understand the relative importance of the terms on the right hand side of the equation as originally proposed in Kang et al. (2001). The terms on the right hand side of Eq. (1) are averaged from surface to 50 m depth to represent the variations in the surface mixed layer of the ocean. These terms are computed from the monthly mean CFSR datasets. It may be noted that the terms on the right hand side of Eq. 1 are computed for the JJA season.

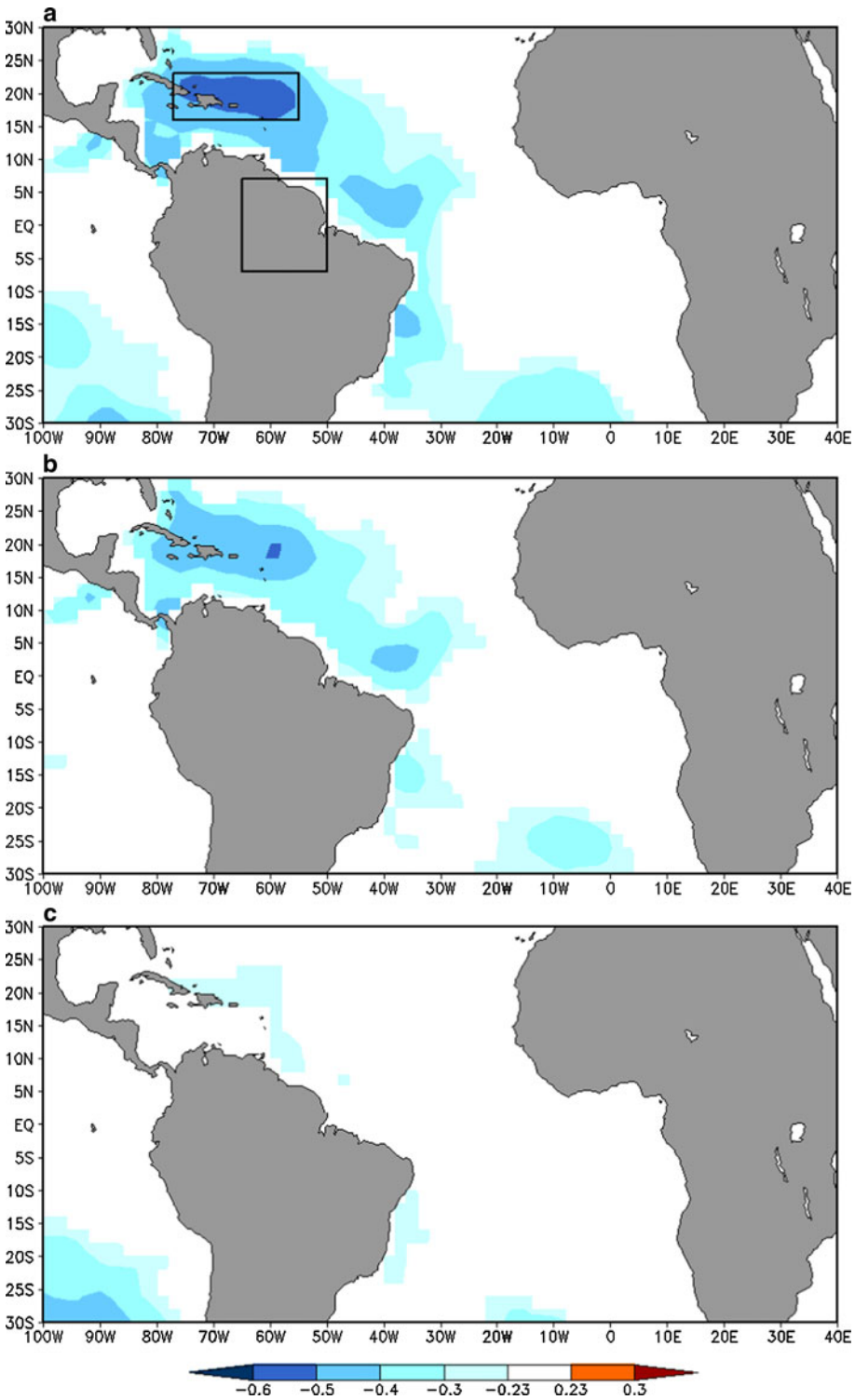

Fig. 1 The correlation of the mean boreal summer (JJA) seasonal SST anomalies with the **a** mean preceding December-January–February (DJF) rainfall, **b** the ENSO component of the preceding DJF rainfall and **c** the rest of the components of the preceding DJF rainfall besides ENSO from Climate Research Unit (CRU) over Equatorial Amazon (7°S–7°N and 65°W–50°W). These correlations are computed over the period from 1950–2004. Only significant values at 90 % confidence interval according to *t* test are shown. The linear trends in rainfall and SST are removed before the correlation is calculated. The reference box over the Caribbean Sea, the core region of the IAS and the EA are outlined in (**a**)

To understand the relative importance of each of the terms on the right hand side of Eq. (1) we compute a standard covariance (SCOV) with the tendency of the SSTA (or left hand side of Eq. 1). The standardized covariance is defined as:

$$SCOV = \frac{COV\left(\frac{\partial T'}{\partial t}, F\right)}{\sigma\left(\frac{\partial T'}{\partial t}\right)} \tag{2}$$

Here, COV stands for covariance and F represents any one of the forcing terms on the right hand side of Eq. (1).

The denominator of Eq. (2) refers to the standard deviation of the time tendency of the SSTA. In this way SCOV will provide the actual magnitude of F that is related to the time series of the tendency of the SSTA. In our case we computed the SCOV for each of the forcing terms with time tendency of the SSTA averaged over the Caribbean Sea, the core of the IAS (outlined in Fig. 1a).

We also make use of Ensemble Empirical Mode Decomposition (EEMD; Wu and Huang 2009; Wu et al. 2011) for decomposing the time series of rainfall over EA to discern the ENSO component. EEMD is a noise assisted data analysis technique that most un-ambiguously discerns the temporal variations through intrinsic mode functions, which are determined by the time series itself rather than from any pre-determined kernels.

4 Results

4.1 The teleconnection

The correlation of the DJF seasonal rainfall over EA with the following JJA seasonal SST variation is shown in Fig. 1a. The negative correlation over the IAS region would suggest that an anomalously wet DJF season over EA is associated with cooler than normal SST over the IAS region in the following JJA season. It is rather intriguing that this correlation is so robust at two season lags. As mentioned earlier most of the earlier studies have dwelled on the boreal spring season SST variability in the North tropical Atlantic Ocean whose sources are an intrinsic component (Giannini et al. 2001, 2004) and the remote ENSO forcing (Enfield and Mayer 1997; Saravanan and Chang 2000). Here, the correlation in Fig. 1a reflects the IAS SST variation in the boreal summer season. It is seen from comparing Fig. 1b and c that the ENSO component of the austral summer EA rainfall has a significant bearing on the EA-IAS teleconnection (Fig. 1a). Through EEMD we isolate the rainfall variability over EA in the 2–7 year time scale. We then regress that component of rainfall on global SST (not shown), which shows the largest regression coefficients in the Niño3 region that reconfirms the isolation of the ENSO forced component of the EA rainfall. Fig. 1c shows that the teleconnection with the IAS SSTA is lost when the correlations are computed from the reconstructed austral summer season rainfall over EA that contain all its temporal components except the ENSO forced component.

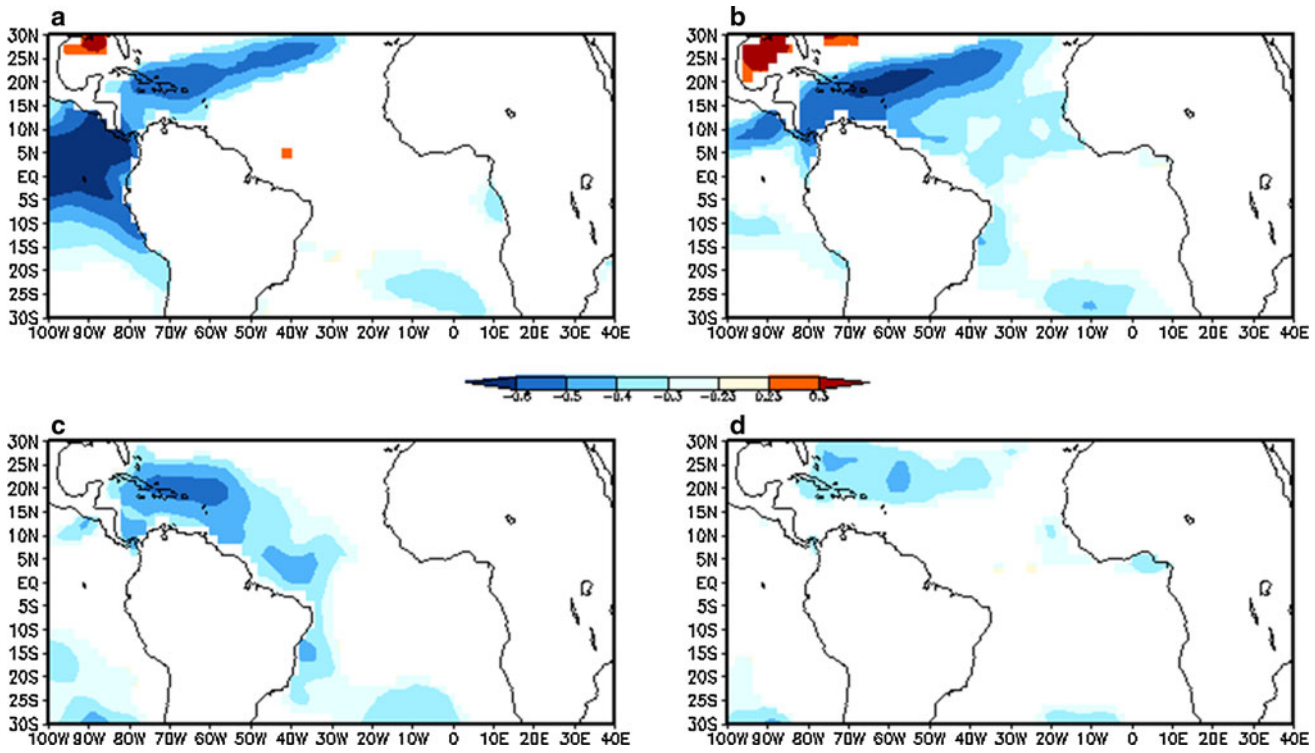

Fig. 2 The correlation of the mean December-January–February (DJF) rainfall over Equatorial Amazon (7°S–7°N and 65°W–50°W) from CRU with the **a** contemporaneous DJF, **b** following March–April–May, **c** following June–July–August (JJA), and **d** following September–October–November (SON) SST from ERSSTv3. Only the significant values at 90 % confidence interval according to *t* test are shown

The teleconnection in Fig. 1a is examined in other seasons in Fig. 2. From Fig. 2 it is apparent that the teleconnection is strongest in March–April–May (Fig. 2b) and then begins to weaken in JJA (Fig. 2c) and further weaken in September–October–November (SON; Fig. 2d). It is most intriguing to see this teleconnection to be so robust in JJA because in the earlier season of MAM, the direct influence of ENSO on the Caribbean Sea is well documented (Enfield and Mayer 1997; Saravanan and Chang 2000). And the teleconnection in the subsequent season of SON (Fig. 2d) also seems to stem largely from the direct influence of the eastern equatorial Pacific through the biennial component of ENSO that has a strong seasonality (Michael et al. 2012). In fact Reihl (1954) points to the existence of the biennial variation of rainfall in the Caribbean region, which in addition to being externally forced by ENSO could also be intrinsic to the region. In Fig. 3 the correlation of the EA austral summer season rainfall with the depth of the 26 °C isotherm is shown. This is a good measure of the ocean heat content in the region required to sustain atmospheric convection, especially that related to tropical cyclones (Shay et al. 2000). The negative correlations over the Caribbean Sea, which begin to appear in MAM and strengthen further into the SON season, suggest that anomalous wet season over EA results in reduced upper ocean heat content in the IAS in the subsequent seasons. These figures also suggest that the SSTA from the surface in DJF (Fig. 2) slowly propagating deeper in the upper ocean over longer seasonal lags (Fig. 3). It may also be noted that in JJA (Fig. 3c) and in SON (Fig. 3d) the simultaneous appearance of the strong negative correlation over eastern equatorial Pacific Ocean and over IAS also suggests the influence of the biennial component of ENSO.

4.2 SSTA over the core of the IAS

In order to understand the teleconnection in Figs. 1, 2, 3, we first need to understand the important forcing mechanisms for the generation of the SSTA in the IAS region. For this we compute the SCOV described earlier for the SST tendencies averaged over a region centered over the Caribbean Sea (outlined by rectangular box in Fig. 1a), which encloses the region with the strongest correlation in MAM and JJA (Figs. 1a, b, 2b, c). In Fig. 4 we show the SCOV of all the dynamical forcing (ocean advection) terms in the right hand side of Eq. (1) for JJA season. Over the Caribbean Sea, none of these dynamical terms seem to contribute to the tendency of SSTA significantly. A similar conclusion can be drawn for other seasons in DJF, MAM,

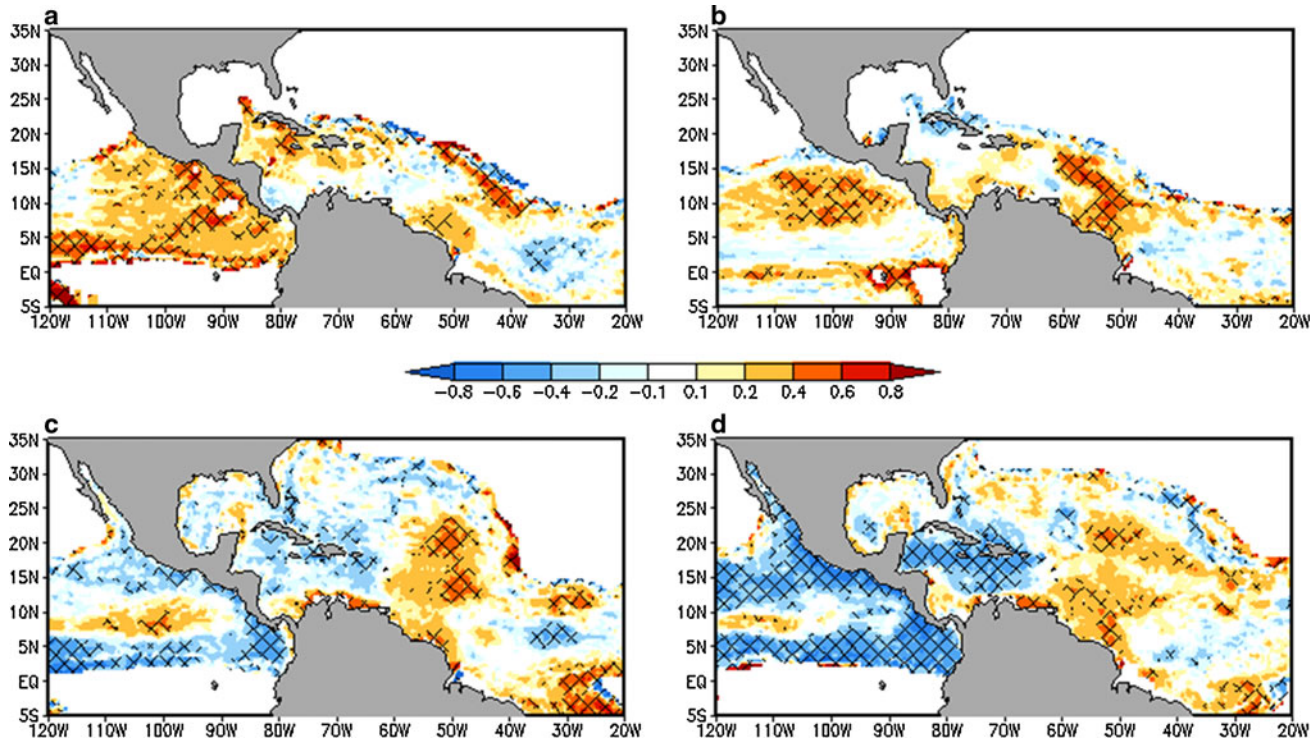

Fig. 3 The correlation of the mean December–January–February (DJF) rainfall over Equatorial Amazon (7°S–7°N and 65°W–50°W) with the **a** contemporaneous DJF, **b** following March–April–May, **c** following June–July–August (JJA), and **d** following September–October–November (SON) 26 °C isotherm depth from CFSR. The significant values at 90 % confidence interval according to *t* test are hashed

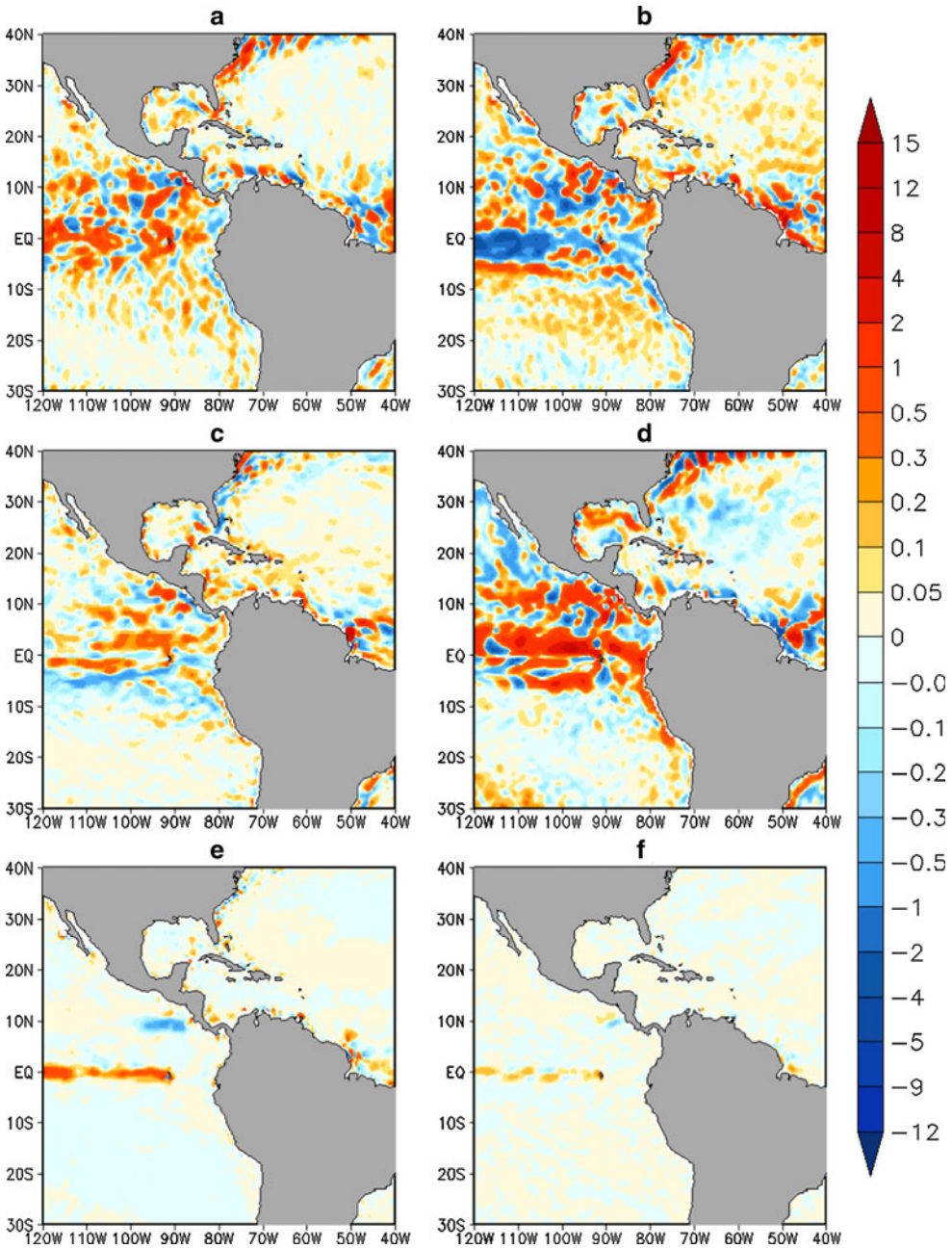

Fig. 4 The standardized covariance (see text for definition) of the SST tendency averaged over the reference box over the Caribbean Sea (see Fig. 1) with **a** $-u_c \frac{\partial T'}{\partial x}$, **b** $-u' \frac{\partial T'}{\partial x}$, **c** $-v_c \frac{\partial T'}{\partial y}$, **d** $-v' \frac{\partial T'}{\partial y}$, **e** $-w_c \frac{\partial T'}{\partial z}$, and **f** $-w' \frac{\partial T'}{\partial z}$averaged over a depth of 50 m from the surface from CFSR for the June–July–August season. The units are in °C month^{-1}

and SON (not shown). However the SCOV with the net heat flux (Fig. 5a) for JJA season indicates that the net heat flux is a relatively much stronger forcing term than any of the dynamical terms. Here a negative covariance suggests that the warming tendency of the SSTA over the Caribbean Sea is accompanied by increased net heat flux into the ocean (or decreased net heat flux out of the ocean). Similarly the SCOV with the component terms of net heat flux including latent heat flux (Fig. 5b), sensible heat flux (Fig. 5c), net short wave flux at surface (Fig. 5d), and net long wave flux at surface (Fig. 5e) indicate that the latter two radiative forcings are the strongest forcing terms. In other words, Fig. 5d and e indicate that the warming tendency of the SSTA over the Caribbean Sea is associated with a concomitant increase in downwelling shortwave flux and a reduction in upwelling long wave flux at the surface respectively. It may be noted that the relative contributions of these fluxes change with season. For example in DJF, the contribution of the latent heat flux is stronger than in JJA (not shown). However, it is sufficient to state that the net heat flux is a dominant forcing term of the tendency of SSTA in the Caribbean Sea in the DJF, MAM, JJA, and SON seasons. The predominance of the surface radiative forcing on the Caribbean SSTA is also consistent with Wang and Enfield (2001). However as noted in Misra et al. (2009), despite the relatively weaker forcing of the

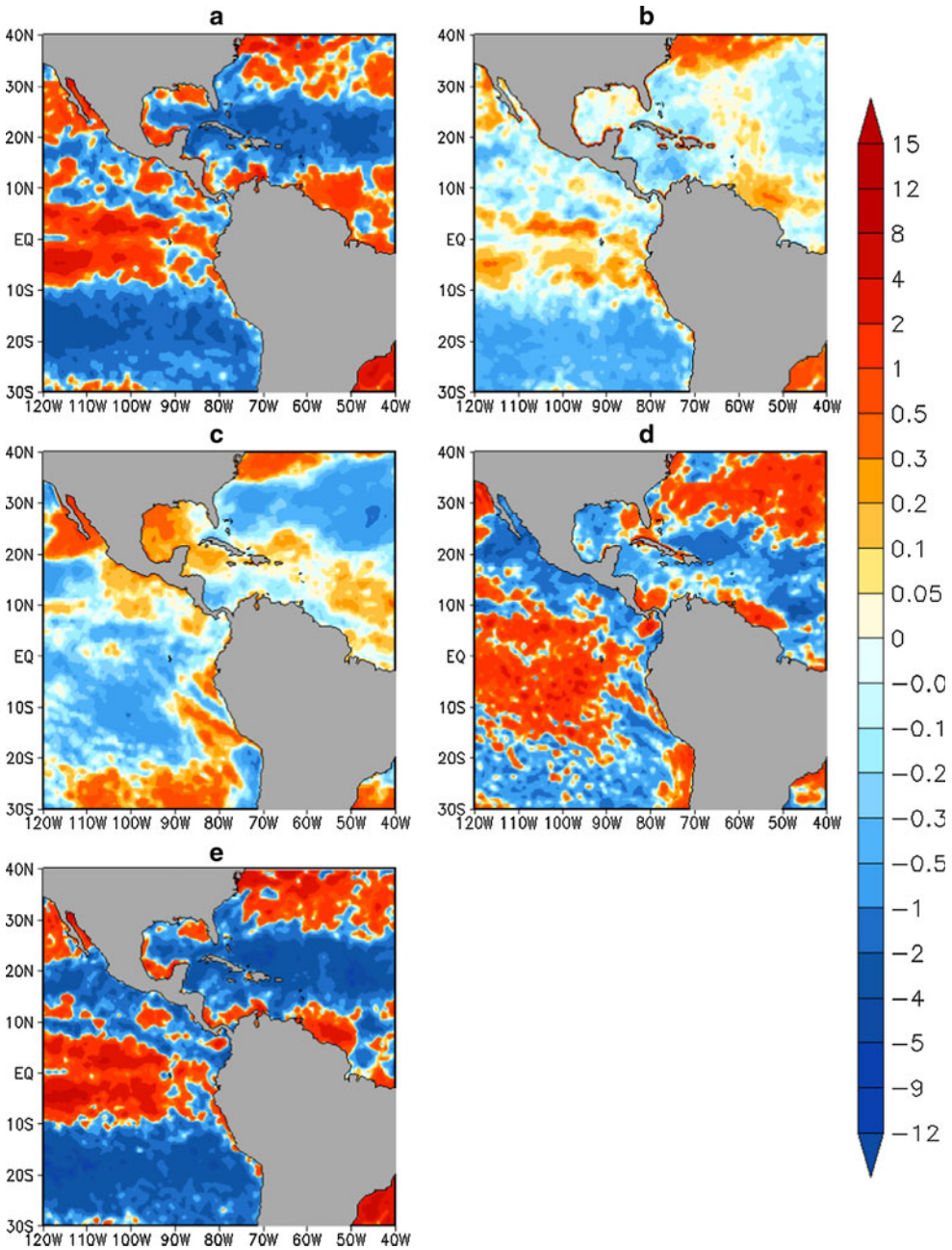

Fig. 5 Same as Fig. 4 but the standardized covariance of the SST tendency averaged over the reference box over the Caribbean Sea (see Fig. 1) with **a** net heat flux, **b** latent heat flux, **c** sensible heat flux, **d** net shortwave flux at surface, and **e** net longwave at surface. Here the surface fluxes are positive when they are directed upward from the ocean to the atmosphere

evaporative fluxes in the boreal summer over the IAS, the absence of air-sea coupling in a climate model (as in a two tiered atmospheric general circulation model forecast setup) leads to misrepresentation of the latent heat flux and the rainfall-SST relationships over the IAS region.

In a related study, Lee et al. (2007), using the output from an ocean general circulation model, diagnosed that the annual cycle of the IAS is dictated largely by the monotonic increase of the clear sky radiation flux from December to May and then its subsequent decline by the end of the year. They also found from the same heat budget analysis of the ocean model simulation that in the Caribbean Sea region, the amplitude of the annual cycle is relatively weakened by the horizontal advection of cold water by the Caribbean current from the upwelling regions of northern South America and turbulent mixing induced by the relatively strong vertical shear of the Caribbean current. In this study however, we are examining the interannual variations of the SSTA in the IAS, and specifically over the Caribbean Sea region.

4.3 The relationship of EA rainfall with SSTA forcing terms

The correlation of the DJF rainfall over EA with net heat flux at the surface for the four seasons is shown in Fig. 6.

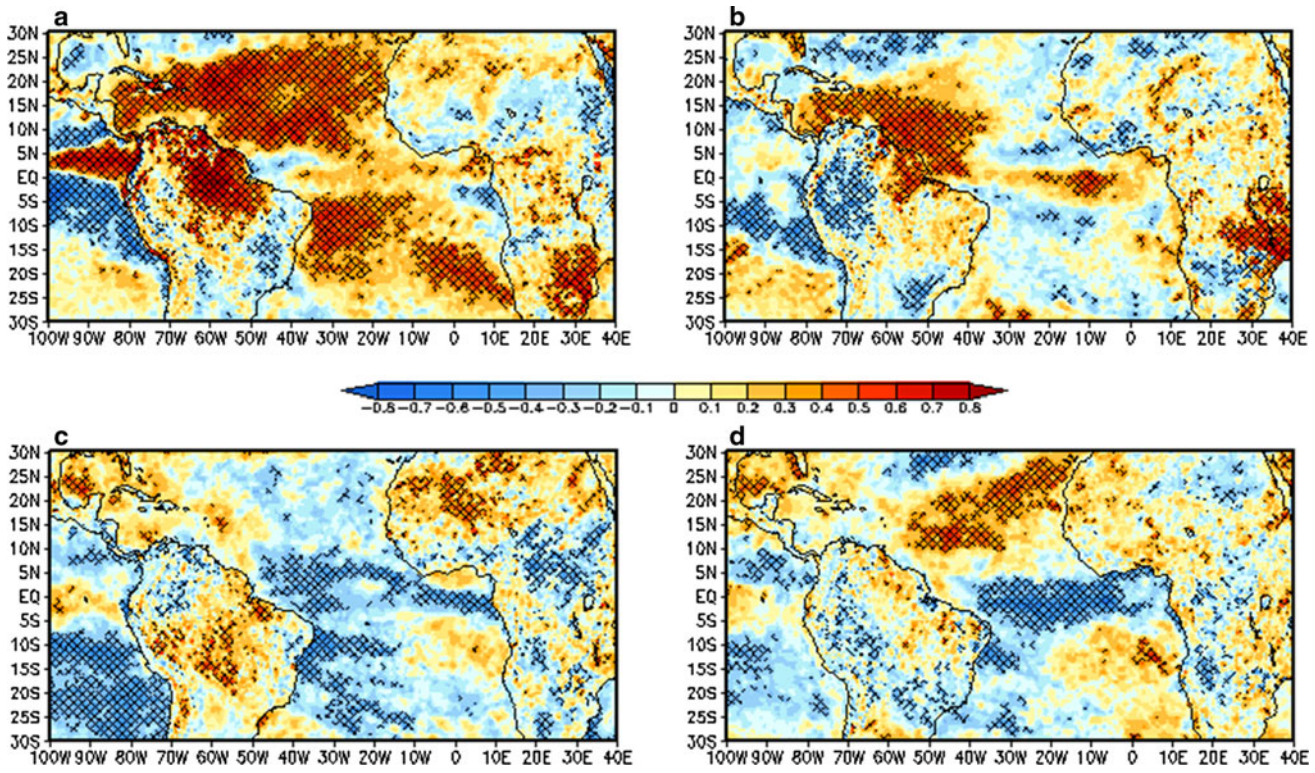

Fig. 6 The correlation of the mean December–January–February (DJF) rainfall over Equatorial Amazon (7°S–7°N and 65°W–50°W) with the **a** contemporaneous DJF, **b** following March–April–May, **c** following June–July–August (JJA), and **d** following September–October–November (SON) net heat flux at surface from CFSR. Here again, the surface fluxes are considered positive when upward from ocean to atmosphere. The significant values at 90 % confidence interval according to *t* test are hashed

The strong positive correlations in Fig. 6a over the IAS indicate that in an anomalously wet DJF there is a very strong corresponding decrease in the net heat flux into the IAS, which perpetuates in the subsequent seasons of MAM (Fig. 6b), JJA (Fig. 6c) and SON (Fig. 6d) but with a lesser influence as indicated by the decreasing correlations. In an anomalously wet DJF over EA, the strong northeasterly flow increases the surface evaporation from the underlying ocean surface (Fig. 7a), which largely drives the reduction of the net heat flux over the IAS as in Fig. 6a. In the subsequent seasons, the influence of the DJF rainfall over EA on the northeasterly flow eases with a concomitant reduction in the influence of the latent heat flux (Fig. 7b–c), and slowly the radiative fluxes begin to dominate (Fig. 8).

Initially in DJF there is a reduction of the upwelling longwave flux from the southern IAS with an anomalous increase in rainfall over EA (Fig. 8a). But in subsequent seasons (Fig. 8b–d) the upwelling longwave flux increases with the anomalously wet DJF season over EA. This behavior of the teleconnection of the DJF rainfall over EA with upwelling longwave fluxes over IAS is consistent with the teleconnection of precipitable water (Fig. 9). In a wet DJF over EA there is an associated increase in precipitable water over IAS (Fig. 9a). This increase in precipitable water is likely sustained from the increased evaporation off the ocean surface associated with the strong low level northeasterly flow in the region (Fig. 7a). However, in the subsequent seasons, the modulation of the evaporation from the ocean surface due to EA rainfall variability eases (Fig. 7b–d), which consequently reduces the moisture in the atmospheric column, thereby raising the net upwelling longwave flux over IAS (Fig. 8b, c). From our earlier analysis this modulation of the surface longwave flux will have the strongest influence on the SSTA in the Caribbean Sea in seasons subsequent to DJF. It may be noted that by SON the influence of the DJF rainfall over EA on precipitable water over IAS reduces significantly. The influence of the DJF rainfall over EA on the net shortwave flux over IAS (Fig. 10) is relatively less significant than that over the net upwelling longwave flux, especially in the JJA season (Fig. 10c).

5 Discussion

The important missing link to explain this teleconnection is the mechanism by which the austral summer rainfall

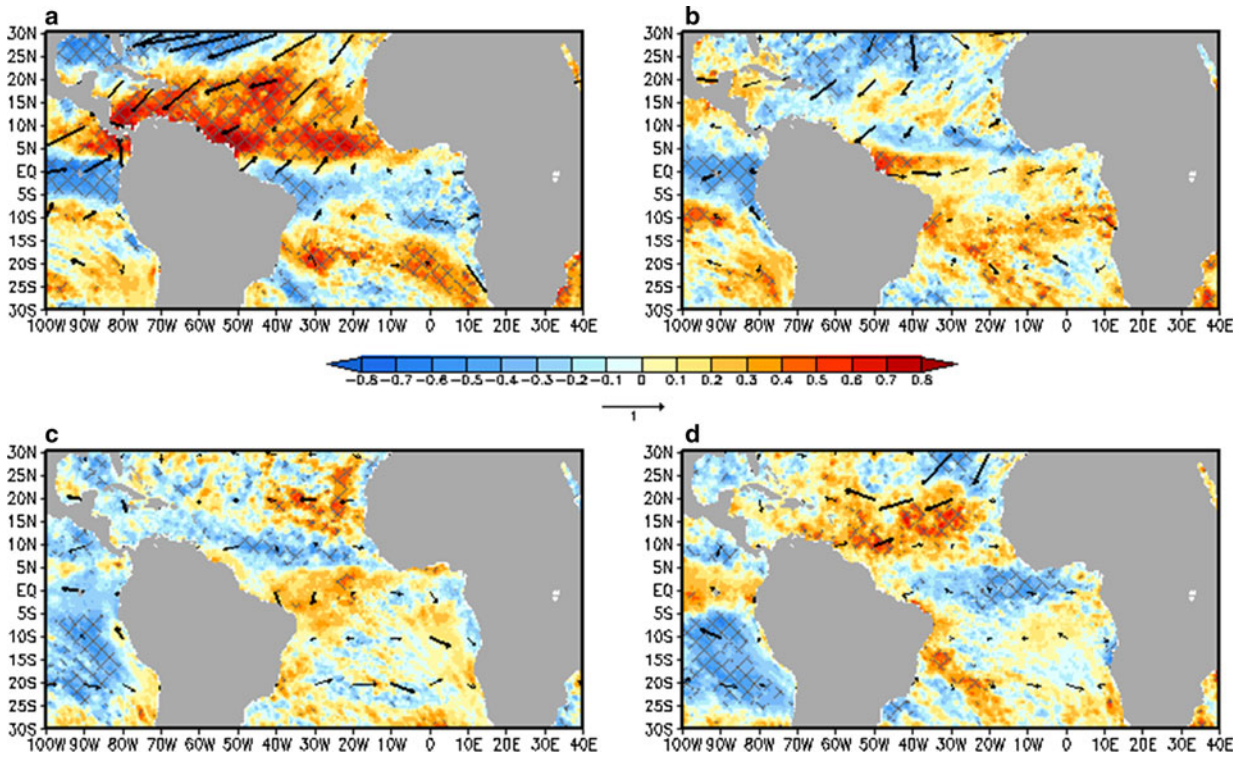

Fig. 7 The linear correlation (regression) of the mean DJF rainfall over Equatorial Amazon (7°S–7°N and 65°W–50°W) on the mean **a** DJF (0 lag), **b** MAM (1 season lag), **c** JJA (2 season lag), and **d** SON (3 season lag) with surface evaporation (850 hPa mean winds) from the CFSR. Significant values at 10 % significance level are hashed for surface evaporation and vectors are made *bold*

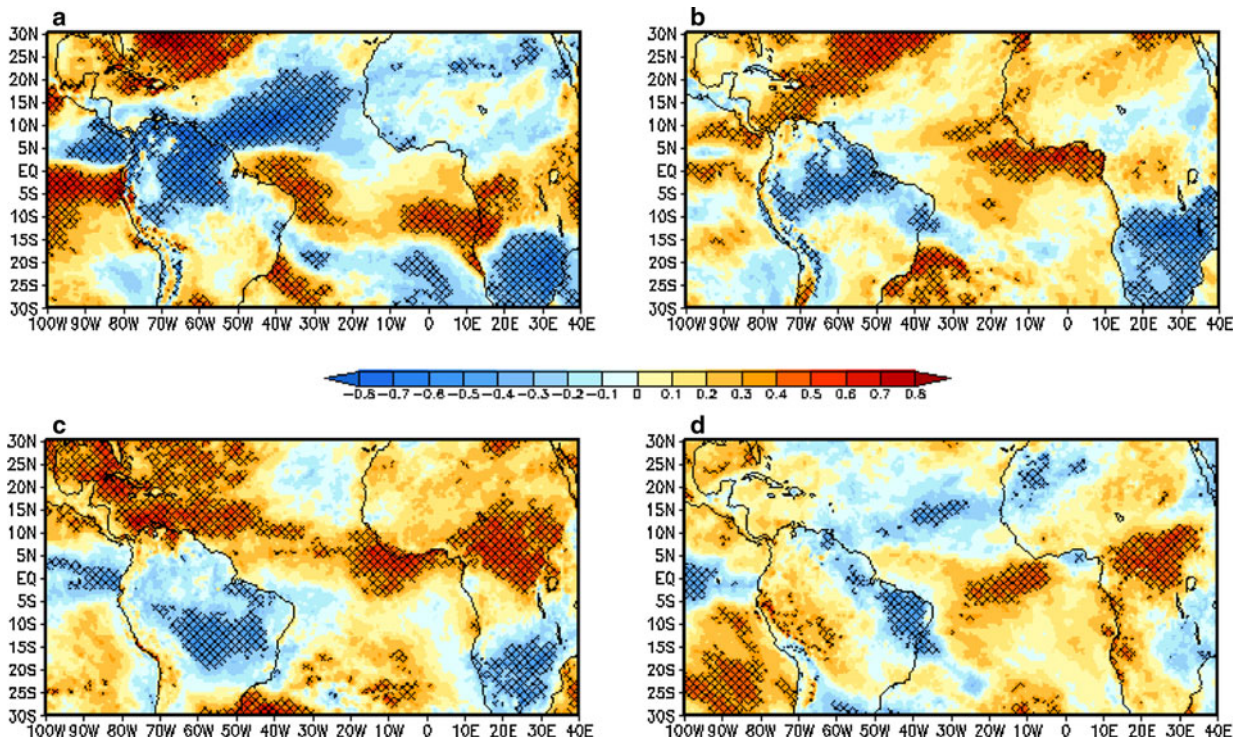

Fig. 8 Same as Fig. 6 but the correlation of the mean December–January–February (DJF) rainfall over Equatorial Amazon (7°S–7°N and 65°W–50°W) with the **a** contemporaneous DJF, **b** following March–April–May, **c** following June–July–August (JJA), and **d** following September–October–November (SON) net longwave flux at the surface from CFSR

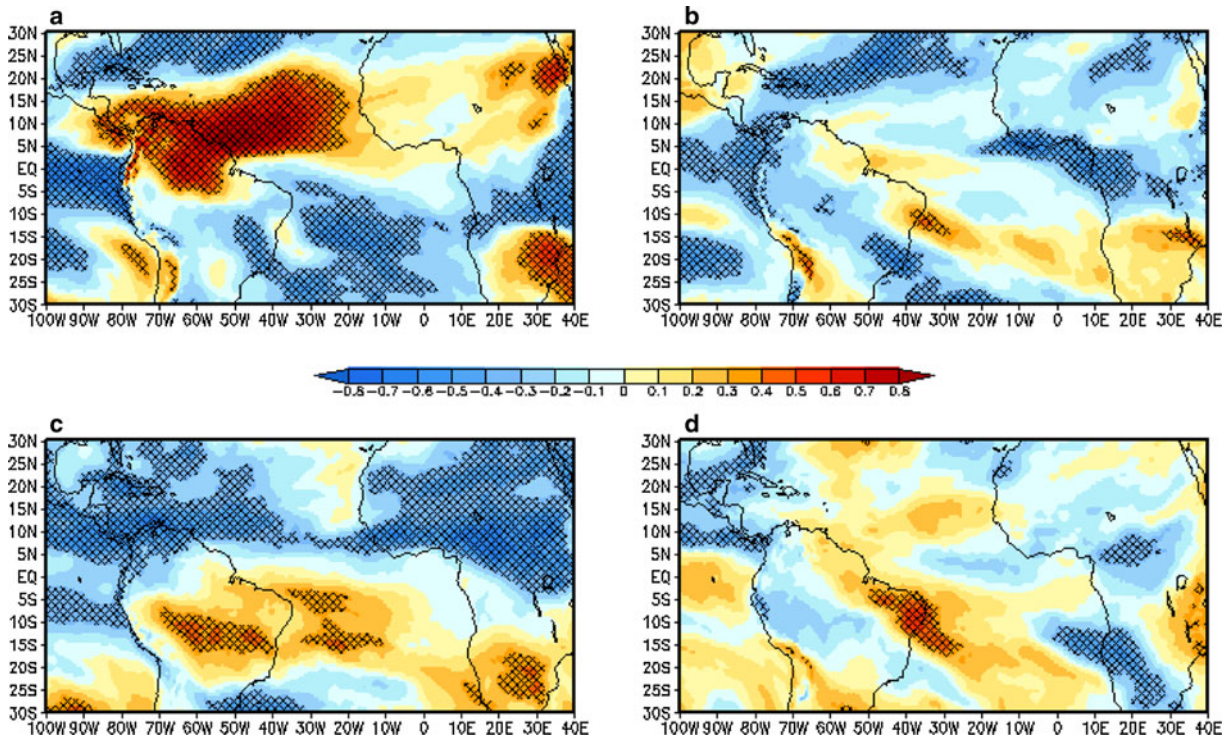

Fig. 9 The correlation of the mean December–January–February (DJF) rainfall over Equatorial Amazon (7°S–7°N and 65°W–50°W) with the **a** contemporaneous DJF, **b** following March–April–May (MAM), **c** following June–July–August (JJA), and **d** following September–October–November (SON) precipitable water from CFSR. The significant values at 90 % confidence interval according to *t* test are hashed

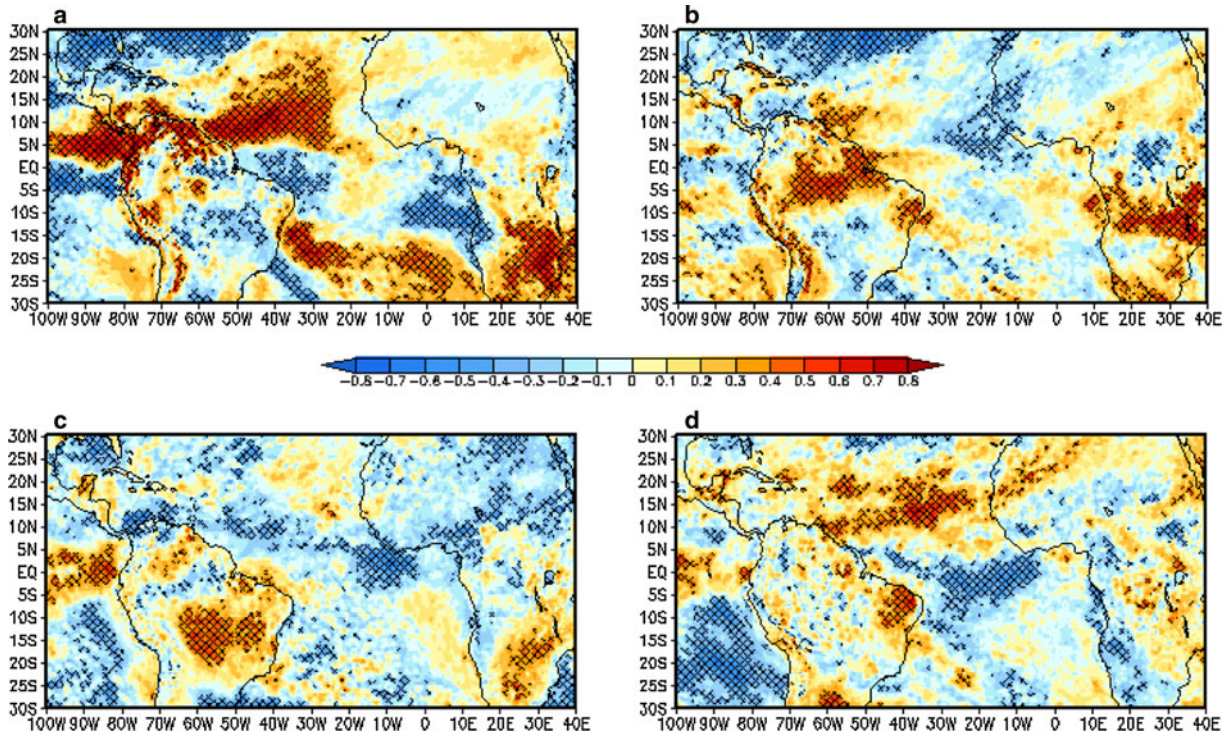

Fig. 10 Same as Fig. 6 but the correlation of the mean December–January–February (DJF) rainfall over Equatorial Amazon (7°S–7°N and 65°W–50°W) with the **a** contemporaneous DJF, **b** following March–April–May, **c** following June–July–August (JJA), and **d** following September–October–November (SON) net shortwave flux at surface from CFSR

dictates the modulation of the precipitable water in the IAS region. It may be noted that in wet EA years, the precipitable water over IAS in the subsequent MAM, JJA, and SON seasons is reduced appreciably, which then reflects in the increased upwelling longwave flux.

To ascertain this mechanism we resort to composite analysis. We composite rainfall (from CMAP) and surface convergence anomalies (computed at 1,000 hPa from CFSR) for the 5 wettest (Fig. 11) and 5 driest (Fig. 12) DJF years recorded from 1979 to 2004. It is observed from the composite anomalies in Fig. 11 that in anomalously wet DJF years over EA, the Atlantic ITCZ is further south than climatology in all four seasons. More importantly, it is notable that the descending limb of the local Hadley cell associated with the western Atlantic ITCZ (that can be discerned by the zonal band of anomalous dry region and surface divergence) is centered around the Caribbean Sea in MAM (Fig. 11b) and JJA (Fig. 11c) in wet EA years. In fact the core region of the IAS (outlined in Fig. 11c) is almost co-located with the descending regions of the anomalous Hadley cell in wet EA years. In dry EA years however, the Atlantic ITCZ location is northward in location relative to climatology in all seasons (Fig. 12). It is apparent in Fig. 12c (JJA season) that the ascending cell of the anomalous Hadley cell in dry EA years is nearly co-located with the core region of the IAS (outlined in the figure). In this situation during dry EA years, when the ascending portions of the anomalous Hadley cell is located over the IAS, the in situ precipitable water is bound to increase that would entail in the reduction of the upwelling longwave flux and a rise in the SSTA. As mentioned earlier, the dominance of the upward longwave flux in regulating the SSTA over IAS will overcome the effect of the concomitant reduction in the upwelling shortwave flux at the surface of the IAS from the increase in cloud cover during dry EA years.

Wang and Enfield (2003) in their diagnostic study with atmospheric reanalysis allude to the seasonal movement of the atmospheric diabatic heat source and associated overturning circulations of the atmosphere to explain the seasonality of the WHWP. They then further suggest that development of WHWP subsequent to an El Niño winter sets up anomalous Hadley circulations to sustain itself. Our study supports their findings and in fact forms the basis for our observed teleconnection between the boreal winter EA rainfall variations and boreal summer variations of IAS SSTA.

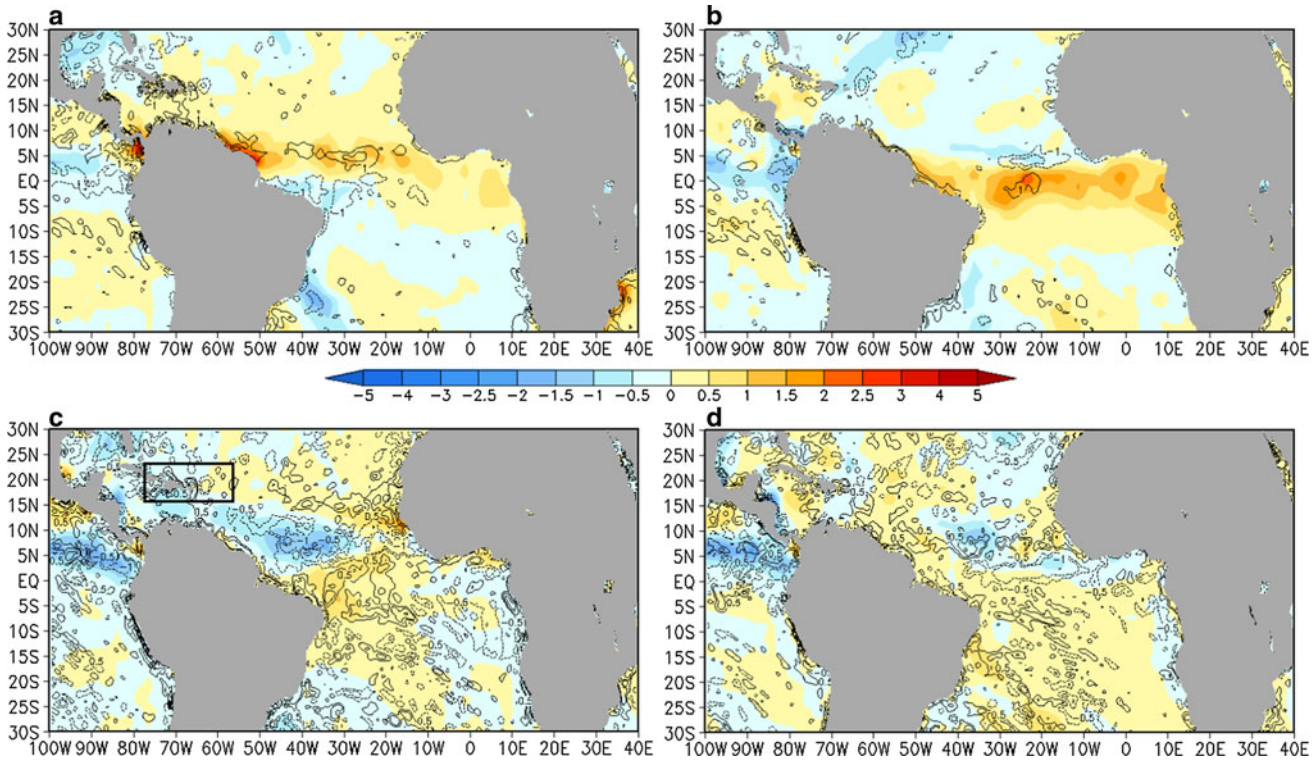

Fig. 11 The composite rainfall anomaly from CMAP (*shaded*; in mm day^{-1}) for the 5 wettest years in DJF over EA recorded between 1979–2004 overlaid with surface (1,000 hPa) convergence (in contour; $\times 10^6$ s) shown only over the oceans for **a** DJF, **b** MAM, **c** JJA, and **d** SON. Positive (negative) surface convergence shown as *solid* (*dotted*) contours signifies surface convergence (divergence). Additional two contours for -0.5×10^{-6} s^{-1} and 0.5×10^{-6} s^{-1} are added in *panels c* and *d*. The outline of the IAS core region from Fig. 1a is repeated in Fig. 11c

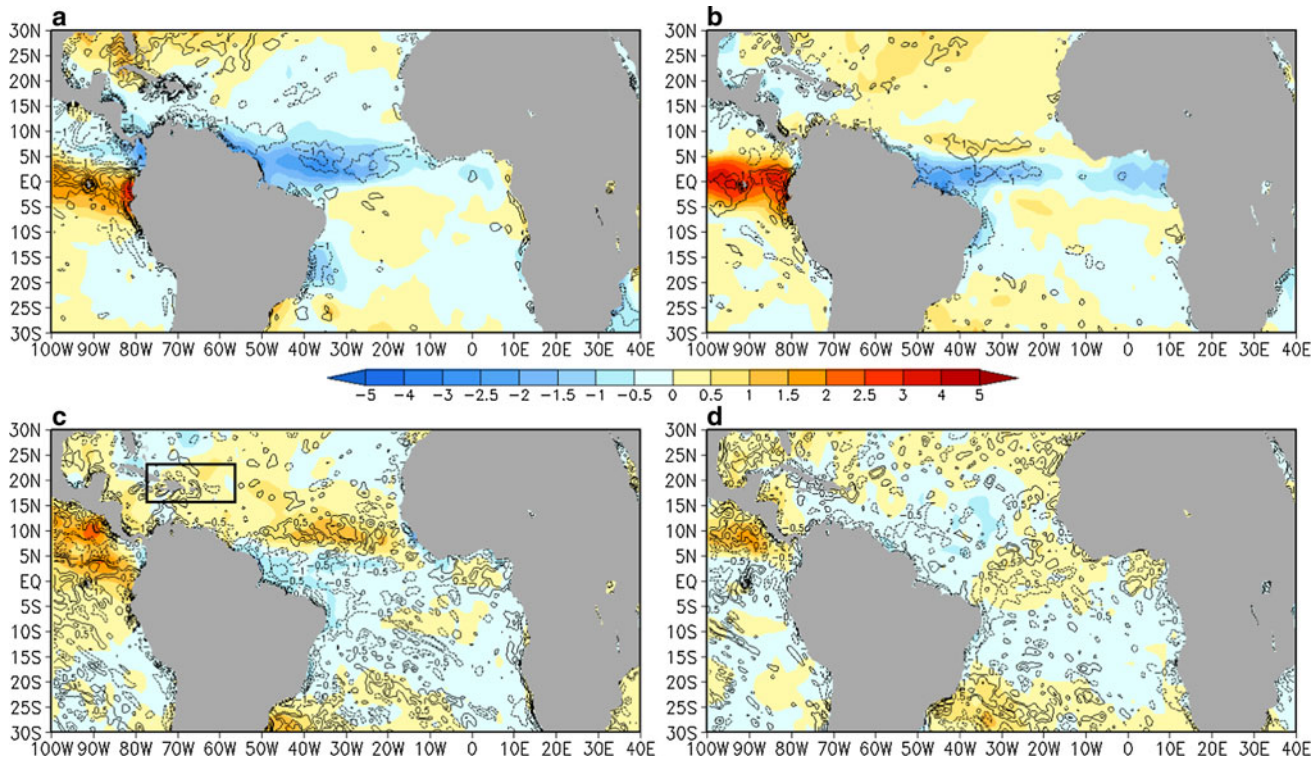

Fig. 12 Same as Fig. 11 but for the 5 driest years in DJF over EA recorded between 1979–2004

6 Conclusions

In this observational study we show a teleconnection between the boreal winter (DJF) seasonal rainfall anomaly over EA and the SSTA over the IAS in DJF (zero lag), MAM (1 season lag), JJA (2 season lag), and even in SON (3 season lag). This teleconnection is primarily stemming from the ENSO component of the EA rainfall anomaly. The teleconnection in JJA is of most interest in this paper as the direct influence of ENSO in late boreal winter and spring seasons are well known from prior studies.

It is discerned from the analysis of the equation for SSTA, that the Caribbean SSTA is strongly influenced by the net surface radiative fluxes in the seasons subsequent to DJF. This helped in isolating the influence of austral summer EA rainfall on these radiative fluxes. It is found that in anomalously wet DJF years over EA the western Atlantic ITCZ moves further southward than climatology, resulting in the desiccation of moisture in the atmospheric column under the descending limb of the associated overturning circulation, which happens to be over the Caribbean Sea region. As a result, the upwelling longwave fluxes in the dry atmosphere are anomalously large, which leads to the cooling of the underlying Caribbean SSTA in an anomalously wet austral summer season over EA. Similarly in anomalously dry DJF years over EA, the Atlantic ITCZ is further northward than climatology, with the portions of the ascending limb of the local Hadley cell located over the Caribbean Sea. As a result, the precipitable water over the Caribbean Sea rises in dry austral summer years over EA. Therefore there is an anomalous reduction in the upwelling long wave fluxes over the Caribbean Sea region in an anomalously dry austral summer over EA leading to the warming of the Caribbean SSTA.

Acknowledgments This work was supported by NOAA grant NA07OAR4310221, CDC grant U01EH000421. Its contents are solely the responsibility of the authors and do not necessarily represent the official views of the acknowledged funding agencies.

References

Chan S, Misra V, Smith H (2011) A modeling study of the interaction between the Atlantic warm pool, the tropical Atlantic easterlies, and the Lesser Antilles. J Geophys Res D00Q02, doi: 10.1029/2010JD015260

Chiang JCH, Sobel AH (2002) Tropical tropospheric temperature variations caused by ENSO and their influence on the remote tropical climate. J Clim 15:2616–2631

Enfield DB, Mayer DA (1997) Tropical Atlantic sea surface temperature variability and its relation to El Nĩno Southern Oscillation. J Geophys Res 102:929–945

Foltz GR, McPhaden MJ (2009) Impact of barrier layer thickness on SST in the Central Tropical North Atlantic. J Clim 22:285–299

Giannini A, Chang JCH, Cane MA, Kushnir Y, Seager R (2001) The ENSO teleconnection of the tropical Atlantic Ocean:

contributions of the remote and local SSTs to rainfall variability in the tropical Americas. J Clim 14:4530–4544
Giannini A, Sarvanan R, Chang P (2004) The pre-conditioning role of tropical Atlantic variability in the development of the ENSO teleconnection: implications for the prediction of the Nordeste rainfall. Clim Dyn 22:839–855. doi:10.1007/s00382-004-0420-2
Kang I-S, An I-S, Jin F-F (2001) A systematic approximation of the SST anomaly equation for ENSO. J Meteor Soc Jpn 79:1–10
Lee S-k, Enfield DB, Wang C (2007) What drives the seasonal onset and decay of the western hemisphere warm pool? J Clim 20:2133–2146
Lee S-K, Wang C, Mapes BE (2009) A simple atmospheric model of the local and teleconnection responses to tropical heating anomalies. J Clim 22(2):227–284
Liebmann B, Marengo J (2001) Interannual variability of the rainy season and rainfall in the Brazilian Amazon Basin. J Clim 14:4308–4318
Mestas-Nunez AM, Enfield DB (2001) Eastern equatorial Pacific SST variability: ENSO and non-ENSO components and their climatic associations. J Clim 14:391–402
Michael JP, Misra V, Chassignet EP, Lu J (2012) Comparison of HYCOM2 and POP models in the CCSM3.0 framework. Part II: ENSO fidelity. Clim Dyn (Submitted)
Mitchell TD, Jones PD (2005) An improved method of constructing a database of monthly climate observations and associated high resolution grids. Int J Climatol 25:693–712
Misra V et al (2011) The influence of Atlantic warm pool on panhandle Florida Sea Breeze. J Geophys Res doi:10.1029/2010JD015367
Misra V, Chan S, Wu R, Chassignet E (2009) Air-sea interaction over the Atlantic warm pool in the NCEP CFS. Geophys Res Lett 36:L15702. doi:10.1029/2009GL038737
Munoz E, Wang C, Enfield D (2010) The intra-Americas springtime sea surface temperature anomaly dipole as fingerprint of remote influences. J Clim 23:43–55
Rauscher SA, Kucharski F, Enfield DB (2010) The role of regional SST warming variations in the drying of Meso-America in future climate projections. J Clim 24:2003–2016. doi:10.1175/2010JCLI3536.1
Reihl H (1954) Tropical meteorology. McGraw Hill, New York 392 pp
Saha S et al (2010) The NCEP climate forecast reanalysis. Bull Am Meteor Soc 91:1015–1057
Saravanan R, Chang P (2000) Interaction between tropical Atlantic variability and El Nĩno southern oscillation. J Clim 13:2177–2194
Shay LK, Gone GJ, Black PG (2000) Effects of a warm oceanic feature on hurricane opal. Mon Wea Rev 128:1366–1383
Smith TM, Reynolds RW, Peterson TC, Lawrimore J (2008) Improvements to NOAA's historical merged land-ocean surface temperature analysis (1880–2006). J Clim 21:2283–2296
Vizy EK, Cook KH (2010) Influence of the Amazon/Orinoco Plume on the summertime Atlantic climate. J Geophys Res 115:D21112. doi:10.1029/2010JD014049
Wang C (2002) Atlantic climate variability and its associated atmospheric circulation cells. J Clim 15:1516–1536
Wang C, Enfield DB (2001) The tropical western hemisphere warm pool. Geophys Res Lett 28:1635–1638
Wang C, Enfield DB (2003) A further study of the tropical western hemisphere warm pool. J Clim 16:1476–1493
Wang C, Lee S-K (2007) Atlantic warm pool, Caribbean low-level jet, and their potential impact on Atlantic hurricanes. Geophys Res Lett 34 doi:10.1029/2006GL028579
Wang C, Enfield DB, Lee S-K, Landsea C (2006) Influences of the Atlantic warm pool on Western Hemisphere summer rainfall and Atlantic hurricanes. J Clim 19:3011–3028
Wang C, Lee S-K, Enfield DB (2008) Climate response to anomalously large and small Atlantic Warm pools during the summer. J Clim 21:2437–2450
Wang C, Lee S-K, Mechoso CR (2010) Interhemispheric influence of the Atlantic warm pool on the Southeastern Pacific. J Clim 23:404–418
Wu ZH, Huang NE (2009) Ensemble empirical mode decomposition: a noise assisted data analysis method. Adv Adapt Data Anal 1:1–41
Wu Z, Huang NE, Wallace JM, Smoliak BV, Chen X (2011) On the time-varying trend in global mean surface temperature. Clim Dyn. doi:10.1007/s00283-011-1128-8
Xie P, Arkin P (1996) Analysis of global monthly precipitation using guage observations, satellite estimates, and numerical model predictions. J Clim 9:840–858